APPLIED GEOPHYSICS, Vol.12, No.1 (March 2015), P. 111-119, 9 Figures.
DOI: 10.1007/s11770-014-0463-z

Application of the double absorbing boundary condition in seismic modeling*

Liu Yang[1,2], Li Xiang-Yang♦[1,2,3], and Chen Shuang-Quan[1,2]

Abstract: We apply the newly proposed double absorbing boundary condition (DABC) (Hagstrom et al., 2014) to solve the boundary reflection problem in seismic finite-difference (FD) modeling. In the DABC scheme, the local high-order absorbing boundary condition is used on two parallel artificial boundaries, and thus double absorption is achieved. Using the general 2D acoustic wave propagation equations as an example, we use the DABC in seismic FD modeling, and discuss the derivation and implementation steps in detail. Compared with the perfectly matched layer (PML), the complexity decreases, and the stability and flexibility improve. A homogeneous model and the SEG salt model are selected for numerical experiments. The results show that absorption using the DABC is considerably improved relative to the Clayton–Engquist boundary condition and nearly the same as that in the PML.
Keywords: Double absorbing boundary condition, numerical modeling, finite-difference method, artificial boundary condition

Introduction

Artificial boundary conditions, modeling accuracy, and numerical dispersion are considered the most important and difficult problems in numerical modeling. Owing to computing resources limitations, the wavefield value can only be calculated in the finite domain. To reduce the effect of boundary reflections on the original wavefield, an artificial boundary is introduced.

Presently, three types of boundary conditions are typically used in seismic modeling: the Clayton–Engquist boundary condition (CEBC) (Clayton and Engquist, 1977), attenuation-based boundary condition (Cerjan et al., 1985), and perfectly matched layer (PML) (Bérenger, 1994). CEBC can well tackle vertical incident waves, but it is unsuitable for waves with a wide incident angle. The attenuation-based boundary condition is not good at absorbing low-frequency signals. Among these approaches, PML is able to acquire the best results but at a high computing cost. With improvements in computer performance, PML has attracted more attention, and many have investigated the method stability (Bécache et al., 2003), calculation efficiency (Gedney, 1996), absorption effect (Komatitsch and Tromp, 2003; Yan and Liu, 2013b), the application domain (Song et al.,

Manuscript received by the Editor September 25, 2014; revised manuscript received November 24, 2014.
*This research is supported by the National Nature Science Foundation of China (Grant No. U1262208) and the Important National Science & Technology Specific Projects (Grant No. 2011ZX05019-008).
1. State Key Laboratory of Petroleum Resources and Prospecting, China University of Petroleum, Beijing 102249, China.
2. CNPC Key Laboratory of Geophysical Prospecting, China University of Petroleum, Beijing 102249, China.
3. Edinburgh Anisotropy Project, British Geophysical Survey, Edinburgh EH9 3LA, UK.
♦Corresponding Author: Li Xiang-Yang (Email: xyl1962@hotmail.com)

2011; Zhao and Shi, 2013) and the propagation medium (Collino and Tsogka, 2001; Yan and Liu, 2013a). PML instability appears in tangential incident waves, or it is expressed as prolonged modeling in complex media such as anisotropic and porous media. The convolutional perfectly matched layer (C-PML) can deal with the instability due to tangential incident waves but at a high computation cost (Roden and Gedney, 2000). Besides these three types of boundary conditions, new boundary conditions are constantly proposed with the aim to reduce complexity and improve flexibility. The most representative boundary condition is the hybrid (Liu and Sen, 2010, 2012). The hybrid absorbing boundary condition introduces a transition zone between the inner region and the boundary to realize the smooth transition between the one-way and two-way wave equations and to eliminate the artificial boundary reflections. However, this boundary condition is constructed on the basis of the classic low-order boundary conditions, e.g., CEBC and Higdon ABC (Higdon, 1987), with second-order precision.

The local high-order absorbing boundary condition (ABC), a method presented by Collino (1993), is equally popular with PML, and it can achieve absorption with any precision order. Each point on the boundary of the local high-order ABC is only related to adjacent points and corresponds to a set of auxiliary variables. The condition can be easily implemented with relatively good absorption effect. The change in the wave equation under PML leads to complex theoretical derivations and is difficult to perform. However, the high-order ABC processes boundary and interior regions separately and thus greatly minimizes computation difficulties. However, the high-order ABC cannot readily treat corners (Rabinovich et al., 2010). Recently, Hagstrom et al. (2014) proposed the double absorbing boundary condition (DABC). This method offers the advantages of the high-order ABC using a finite thickness and avoiding the special treatment of corners. In addition, the DABC improves the absorption effect by increasing either the boundary thickness or the order of precision. Therefore, in contrast to the high-order ABC, it improves flexibility. Simultaneously, the DABC also avoids the instability problems of the PML (Rabinovich et al., 2010).

For efficient and accurate application of the boundary condition in seismic modeling, we opted for the DABC. We performed adaptability analysis of the DABC with finite-difference (FD) methods, then derived the particular form of the DABC by modeling the 2D acoustic wave propagation equation, and discussed the methodology in detail. Then, we modeled a homogeneous and a complex medium separately under different boundary conditions. Finally, the results are summarized in the conclusions.

Method

Basic theory

As in the high-order ABC, the auxiliary variable ϕ_j in the DABC is part of equation (1) (Hagstrom et al., 2014)

$$\begin{cases} a_j\dot{\phi}_j + v\phi_{j,x} + \sigma_j\phi_j = \bar{a}_j\dot{\phi}_{j+1} - v\phi_{j+1,x} + \bar{\sigma}_j\phi_{j+1} \\ 0 < a_j, \bar{a}_j \le 1 \\ \sigma_j, \bar{\sigma}_j \ge 0 \end{cases},$$
$$j = 0, \ldots, P, \tag{1}$$

where P is the order of the absorption accuracy, v is the velocity, and $a_j, \bar{a}_j, \sigma_j, \bar{\sigma}_j$ are the coefficients.

We derive the DABC form that is appropriate for 2D seismic modeling. The 2D acoustic wave equation is

$$\frac{\partial^2 p(x,z,t)}{\partial x^2} + \frac{\partial^2 p(x,z,t)}{\partial z^2} - \frac{1}{v^2(x,z)}\frac{\partial^2 p(x,z,t)}{\partial t^2} = g(t)\delta(x - x_S)\delta(z - z_S). \tag{2}$$

In the above equation, $p(x, z, t)$ is the wavefield. The right-hand expression is the source and (x_s, z_s) is the source position. Figure 1 shows the structure of the CEBC and high-order ABC (Clayton and Engquist, 1977).

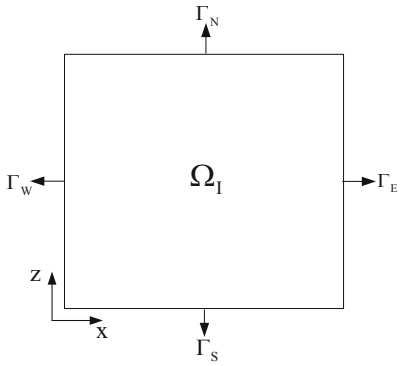

Fig.1 Structure of CEBC and high-order ABC.

In Figure 1, Γ_W, Γ_E, Γ_N,Γ_S represent the west, east, north, and south boundaries, respectively. $\Gamma = \Gamma_W \cup \Gamma_E \cup \Gamma_S \cup \Gamma_N$ denotes the artificial boundary region. Ω_I represents the interior region and the calculation region is $\Omega = \Omega_I \cup \Gamma$. The wavefield is governed by the 2D acoustic wave equation in the interior region, and the wavefield on the

right boundary is governed by the following equation

$$\Gamma_E:\ \partial_t p(x,z,t)+v\partial_x p(x,z,t)=0. \tag{3}$$

The high-order ABC introduces a high-order part in the CEBC, which allows absorption with any order of accuracy. Considering the right boundary Γ_E, e.g., the wavefield on this boundary satisfies equation (4)(5)(6). We substitute $p(x, z, t)$ with p for simplicity

$$(\partial_t+v\partial_x)p=\partial_t\phi_1. \tag{4}$$

$$(\partial_t+v\partial_x)\phi_j=(\partial_t-v\partial_x)\phi_{j+1},\quad j=0,\ldots,P, \tag{5}$$

$$\phi_{P+1}=0. \tag{6}$$

The absorption precision can improve by increasing P (Bécache et al., 2010). A sequence of auxiliary variables $\phi_j = \phi_j(x, y, t)$ is introduced to eliminate the squared items, resulting in the low-order form (Givoli and Neta, 2004).

Equations (5) and (1) are the same when $a_j=\bar{a}_j=1$, $\sigma_j=\bar{\sigma}_j=0$. This set of parameters guarantees the stability and effectiveness of the proposed method.

Figure 2 shows the structure of the DABC. The DABC boundary region Ω_L, where there are variable ϕ_j, includes four inner boundaries (Γ_{IN}, Γ_{IS}, Γ_{IW}, Γ_{IE}), four outer boundaries (Γ_N, Γ_S, Γ_W, Γ_E), and the region between the inner and outer boundaries. In the DABC, high-order ABCs are applied in two parallel FD grids. Ω_I is the interior region, and $\Omega = \Omega_L \cup \Omega_I$ is the calculation region.

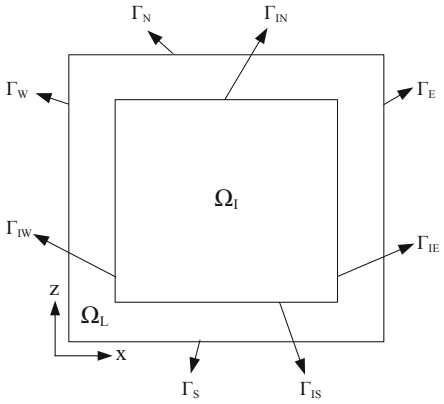

Fig.2 Structure of DABC.

Implementation steps

Here we use the Figure 3 to illustrate the DABC application in acoustic wave equation modeling. The Figure 3a shows a 2D infinite area in the east and west directions. The Figure 3b shows the DABC structure when we set the DABC in the east and the west directions.

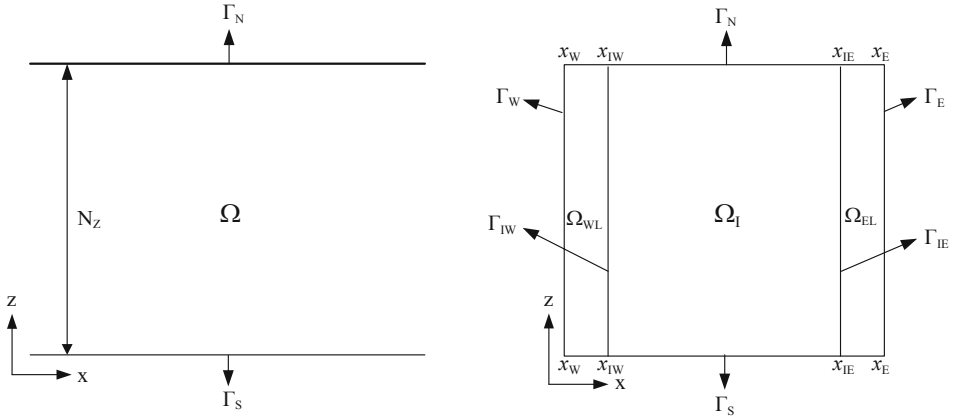

(a) Infinite area in the east and west directions (b) The DABC on east and west directions

Fig.3 Design of DABC.

In the Figure 3, N_z is the gird number in z orientation. The x coordinates of the four high-order absorbing boundaries are x_{IE}, x_E, x_{IW} and x_W. $\Omega_L = \Omega_{WL} \cup \Omega_{EL}$ ($x_{IE} \le x \le x_E \cup \Gamma\ x_W \le x \le x_{IW}$, $0 \le z \le N_z$) is the DABC boundary region. Ω_I represents the interior region and the calculation region is $\Omega = \Omega_L \cup \Omega_I$. ϕ_j satisfy the wave equation and the initial zero conditions, where p is as in equation (2)

$$\begin{aligned}&\phi_j(x,y,t=0)=0,\\&\dot{\phi}_j(x,y,t=0)=0, j=0,..,P+1\ in\ \Omega_L.\end{aligned} \tag{7}$$

The termination conditions are satisfied by ϕ_j on the outer boundaries Γ_W and Γ_E

$$(-v\partial_x + \partial_t)\phi_{P+1} = 0, \tag{8}$$

$$(v\partial_x + \partial_t)\phi_{P+1} = 0. \tag{9}$$

And, on Γ_{IW}, Γ_W, Γ_{IE}, and Γ_E, ϕ_j and ϕ_{j+1} satisfy the recursive relations as in equation (5). The left side of equation (5) is known and the right side of equation (5) is unknown when we calculate the inner boundaries, whereas the right side of equation (5) is known and the left side of equation (5) is unknown when we calculate the outer boundaries.

We use FD discretization for time and space, where dx and dz are the sampling intervals in the x and z directions, respectively. j is the precision order variable. k is the grid number in the x direction. l is the grid number in the z direction. Superscripts j–1, n, and n+1 represent three moments of time in the time order. Discrete operators are defined as follows:

Forward average in space:

$$A_x^+ = (p_{k+1,l} + p_{k,l})/2, \tag{10}$$

Backward average in space:

$$A_x^- = (p_{k-1,l} + p_{k,l})/2, \tag{11}$$

Forward average in time:

$$A_t^+ = (p^{n+1} + p^n)/2, \tag{12}$$

Forward difference in space:

$$D_x^+ = (p_{k+1,l} - p_{k,l})/2, \tag{13}$$

Backward difference in space:

$$D_x^- = (p_{k,l} - p_{k-1,l})/2, \tag{14}$$

Forward difference in time:

$$D_t^+ = (p^{n+1} - p^n)/2. \tag{15}$$

Implementation steps in acoustic wave equation FD modeling with DABC

Step 1. p^n in Ω and ϕ_j^n in Ω_L are given for j = 0, …, P+1.

Step 2 . Compute p^{n+1} in Ω except for Γ_W and Γ_E,

$$p_{k,l}^{n+1} = 2p_{k,l}^n - p_{k,l}^{n-1} + (v\Delta t/h)^2(p_{k+1,l}^n + p_{k-1,l}^n + p_{k,l+1}^n + p_{k,l-1}^n - 4p_{k,l}^n),$$

where h = min (dx, dz).

Step 3. $\phi_j^{n+1} = p^{n+1}$ in Ω_L.

Step 4. Compute ϕ_j^{n+1}(j = 0, …, P+1) for all the interior grid points of Ω_L except Γ_{IW}, Γ_W, Γ_{IE}, and Γ_E

$$\phi_{j,k,l}^{n+1} = 2\phi_{j,k,l}^n - \phi_{j,k,l}^{n-1} + (v\Delta t/h)^n(\phi_{j,k+1,l}^n + \phi_{j,k-1,l}^n + \phi_{j,k,l+1}^n + \phi_{j,k,l-1}^n - 4\phi_{j,k,l}^n).$$

Step 5. Compute ϕ_j^{n+1}(j = P, P–1, …, 0) on the outer boundaries Γ_W and Γ_E with equation (5)

$$A_x^- D_t^+ \phi_{j,W+1,l}^n + vA_t^+ D_x^- \phi_{j,W+1,l}^n = A_x^- D_t^+ \phi_{j+1,W+1,l}^n - vA_t^+ D_x^- \phi_{j+1,W+1,l}^n,$$

$$A_x^+ D_t^+ \phi_{j,E-1,l}^n + vA_t^+ D_x^+ \phi_{j,E-1,l}^n = A_x^+ D_t^+ \phi_{j+1,E-1,l}^n - vA_t^+ D_x^+ \phi_{j+1,E-1,l}^n.$$

The unknown items in the above equations are $\phi_{j,W,l}^{n+1}$ and $\phi_{j,E,l}^{n+1}$. The explicit form is

$$w\phi_{j,W,l}^{n+1} = 2A_x^- D_t^+ \phi_{j+1,W+1,l}^n - 2vA_t^+ D_x^- \phi_{j+1,W+1,l}^n - D_t^+ \phi_{j,W+1,l}^n - vD_x^- \phi_{j,W+1,l}^n + \frac{1}{\Delta t}\phi_{j,W,l}^n + v\frac{\phi_{j,W+1,l}^{n+1}}{\Delta x},$$

$$w\phi_{j,E,l}^{n+1} = 2A_x^+ D_t^+ \phi_{j+1,E-1,l}^n - 2vA_t^+ D_x^+ \phi_{j+1,E-1,l}^n - D_t^+ \phi_{j,E-1,l}^n - vD_x^+ \phi_{j,E-1,l}^n + \frac{1}{\Delta t}\phi_{j,E,l}^n + v\frac{\phi_{j,E-1,l}^{n+1}}{\Delta x},$$

where $w = \frac{1}{\Delta t} + \frac{v}{\Delta x}$.

Step 6 . $p_{W,l}^{n+1} = \phi_{0,W,l}^{n+1}$ and $p_{E,l}^{n+1} = \phi_{0,E,l}^{n+1}$.

Step 7. Compute ϕ_{j+1}^{n+1} (j = 0, …, P) on the inner boundaries Γ_{IW} and Γ_{IE} with equation (5)

$$A_x^- D_t^+ \phi_{j,IW,l}^n + vA_t^+ D_x^- \phi_{j,IW,l}^n = A_x^- D_t^+ \phi_{j+1,IW,l}^n - vA_t^+ D_x^- \phi_{j+1,IW,l}^n,$$

$$A_x^+ D_t^+ \phi_{j,IE,l}^n + vA_t^+ D_x^+ \phi_{j,IE,l}^n = A_x^+ D_t^+ \phi_{j+1,IE,l}^n - vA_t^+ D_x^+ \phi_{j+1,IE,l}^n.$$

The unknown items in the above equations are $\phi_{j,IW,l}^{n+1}$ and $\phi_{j,IE,l}^{n+1}$. The explicit form is

$$w\phi_{j+1,IW,l}^{n+1} = 2A_x^- D_t^+ \phi_{j,IW,l}^n + 2vA_t^+ D_x^- \phi_{j,IW,l}^n - D_t^+ \phi_{j+1,IW-1,l}^n + vD_x^- \phi_{j+1,IW,l}^n + \frac{1}{\Delta t}\phi_{j+1,IW,l}^n + \frac{v}{\Delta x}\phi_{j+1,IW-1,l}^{n+1},$$

$$w\phi_{j+1,IE,l}^{n+1} = 2A_x^+ D_t^+ \phi_{j,IE,l}^n + 2vA_t^+ D_x^+ \phi_{j,IE,l}^n - D_t^+ \phi_{j+1,IE+1,l}^n + vD_x^+ \phi_{j+1,IE,l}^n + \frac{1}{\Delta t}\phi_{j+1,IE,l}^n + \frac{v}{\Delta x}\phi_{j+1,IE+1,l}^{n+1},$$

in which $w = \frac{1}{\Delta t} + \frac{v}{\Delta x}$.

Step 8. $p^n = p^{n+1}$ and $\phi^n = \phi^{n+1}$, then compute p^{n+1}.

Numerical modeling

We designed two groups of FD numerical modeling experiments. The absorption effects of the CEBC, PML, and DABC are compared using three indicators: a snapshot, the wavefield value received at fixed points, and the sum of energy in the entire computational domain.

Homogeneous model

Non-ABC, CEBC, PML, and the proposed DABC are used. As shown in Figure 4, the absorption results of the four boundary conditions are compared for the same conditions. To show the results in different stages of wave propagation, we choose four typical moments at 0.261 s, 0.316 s, 0.386 s, and 0.476 s. The velocity is 2800 m/s, the space sampling interval is 6 m × 6 m, the number of grid points is 251 × 251, and the time step is 1 ms. Twentieth- and second-order regular-grid finite differences are used for spatial and temporal discretization. We use a 30 Hz Ricker wavelet as the source, and the source position is located at the center of the model (750 m, 750 m). The boundary thickness for the PML and DABC is set at ten. The attenuation factor of PML is set at 900. When using the DABC method, modeling with high absorption precision increases the calculation cost. The order P of DABC is set equal to three to achieve the same absorption effect as in the PML. From the snapshots of the third and fourth moments, we find that the CEBC absorbs most of the strong reflection, though some reflected energy remains. However, after the absorption of the PML and DABC, the reflection is nearly eliminated.

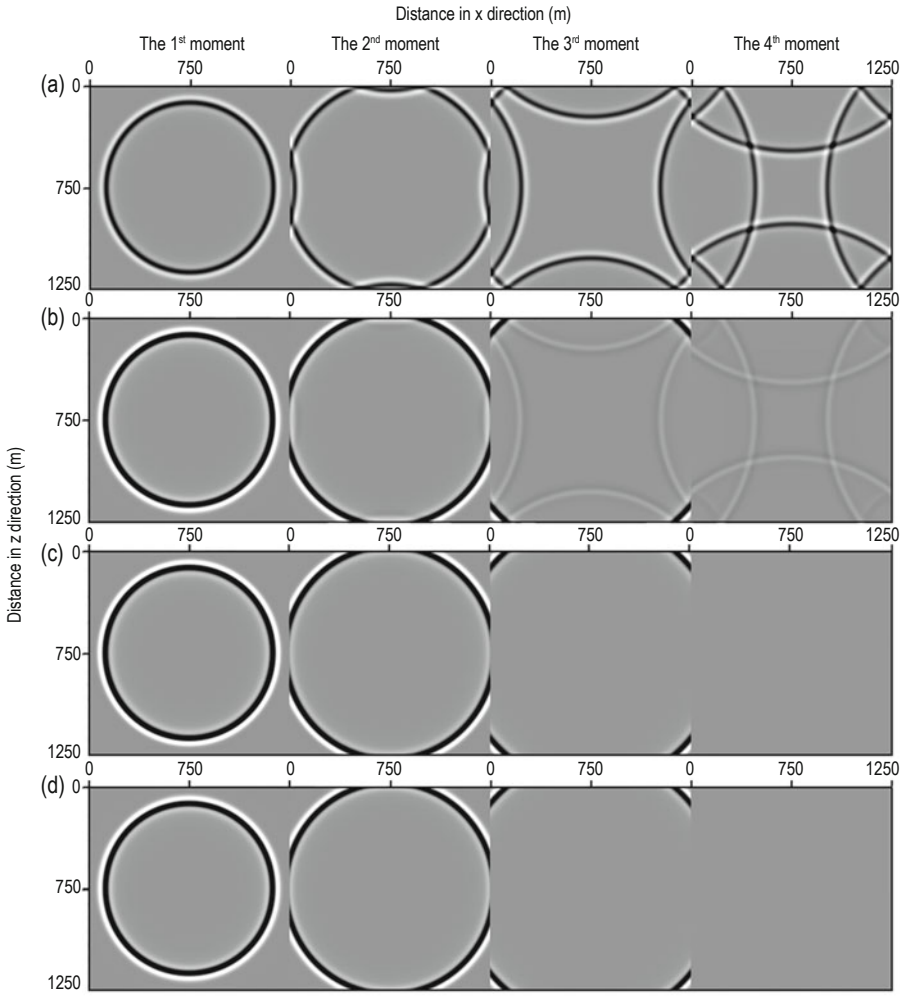

Fig.4 Snapshots at different moments. (a) Non-ABC; (b) CEBC; (c) PML; (d) DABC.

In Figure 5, the direct and reflected waves at (300 m, 750 m) are compared using the aforementioned four methods. In Figure 5a, we find that the direct wave is nearly the same for these four methods, but the differences in the reflected wave are obvious. In the CEBC, some reflected wave energy is still visible, whereas in the PML and DABC, the reflected wave is completely absorbed. Figure 5b shows the comparison of the reflected wave under the DABC and PML, from which we see that the reflected wave energy is negligible when compared with that of the direct wave, and the two boundary conditions have similar effectiveness.

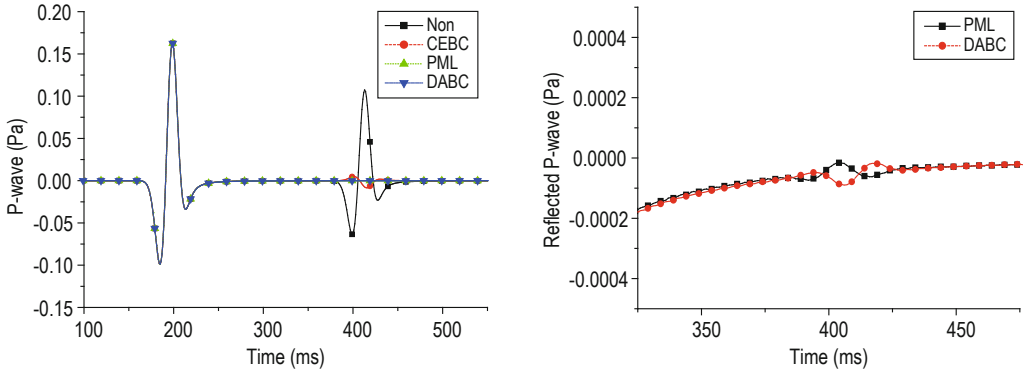

(a) Direct and reflected waves under non-ABC, CEBC, PML, and DABC (b) Reflected wave under DABC and PML

Fig.5 Wavefield values at (300, 750).

Figure 6 show the sum of the energy for different boundary conditions. Figure 6a shows the sum of the wave energy as a function of time. The energy sum of the reflected wave at a later stage is also shown in Figure 6b. The results suggest that the proposed DABC absorbs the reflected wave nearly completely, similar to the PML.

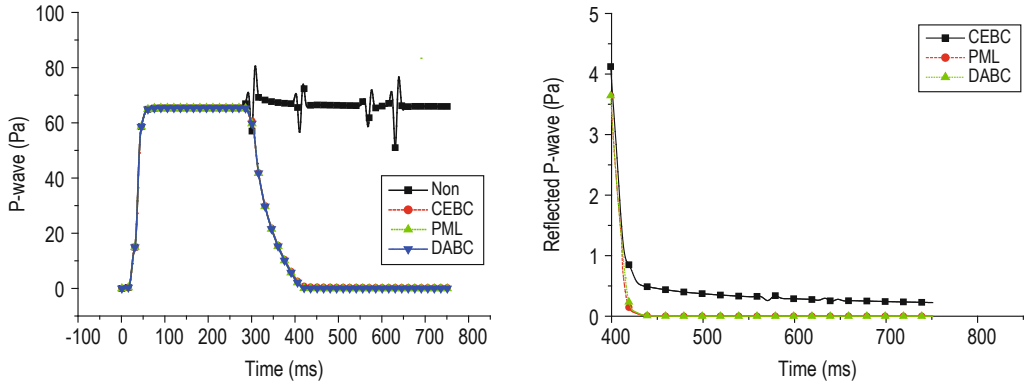

(a) Direct and reflected waves under non-ABC, CEBC, PML, and DABC (b) Reflected wave under DABC and PML

Fig.6 Sum of energy.

SEG salt model

Figure 7 shows the SEG salt model velocities. The number of grid points is 649 × 150, the space sampling interval is 10 m × 10 m, and the time step is 1 ms. Sixteenth- and second-order finite differences are used in the spatial and temporal discretization. We use a 30 Hz Ricker wavelet as the source, and the source position is located at the center of the model surface (3240 m, 0 m). The boundary thickness of the PML and DABC is set at 18. The attenuation factor of PML is set at 800. The DABC order P is set at five to achieve the same absorption precision as in the PML.

Figure 8 shows the FD model seismograms for the SEG salt model for the non-ABC, CEBC, PML, and DABC schemes. Figure 9 shows the details in the red rectangles of Figure 8. A strong boundary reflection

destroys the seismic data under non-ABC. CEBC absorbs some of the boundary reflection but a strong boundary reflection remains. However, there is nearly no boundary reflection for the PML and DABC. The numerical modeling of this complex model shows that the DABC effectively absorbs the boundary reflection. The absorption of the DABC is much better than that of the CEBC, and almost the same as the classic PML.

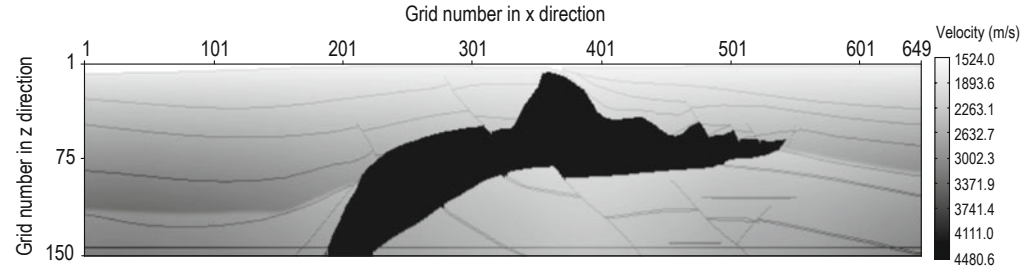

Fig.7 SEG salt model.

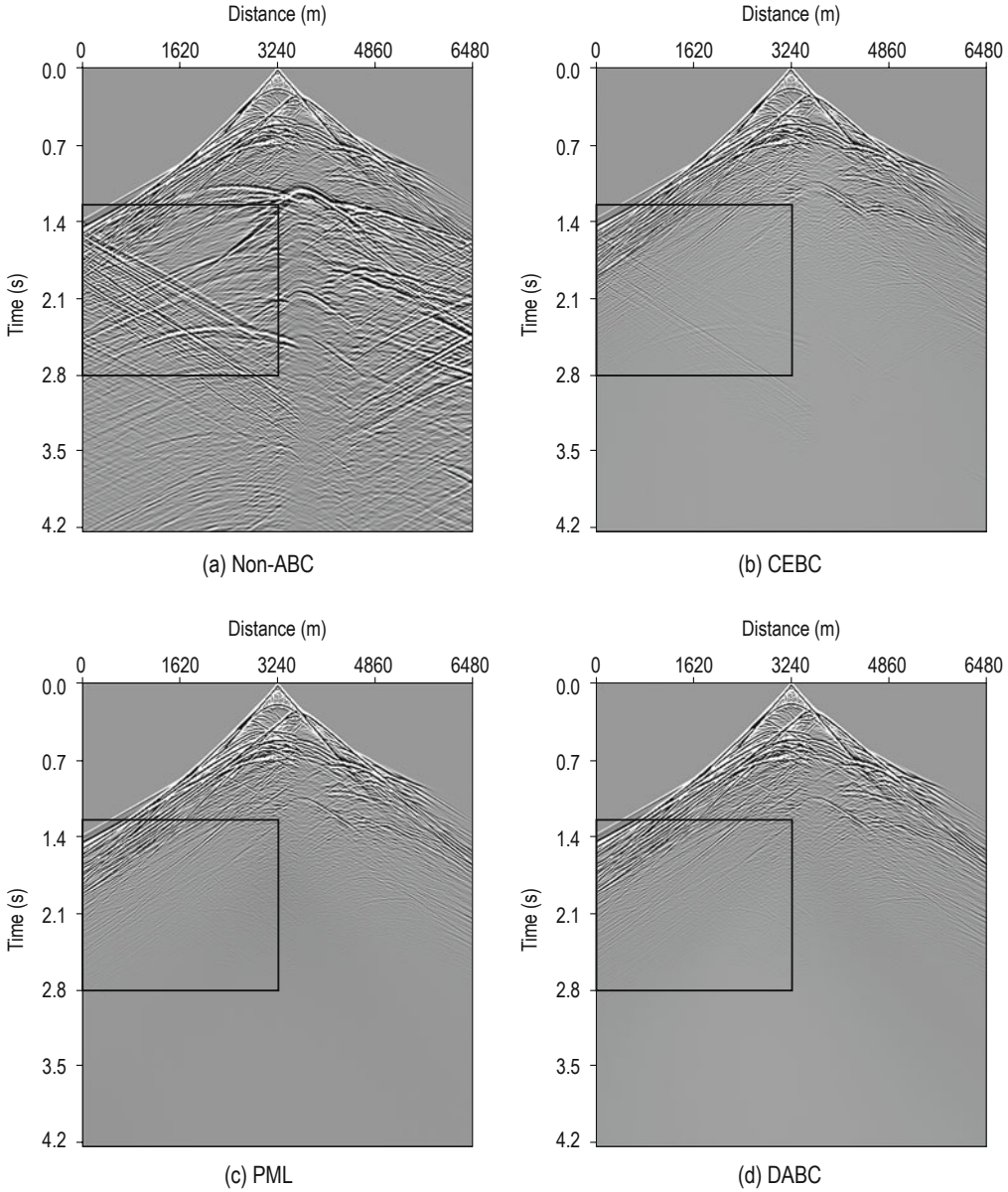

Fig.8 Seismograms for SEG salt model for different boundary conditions.

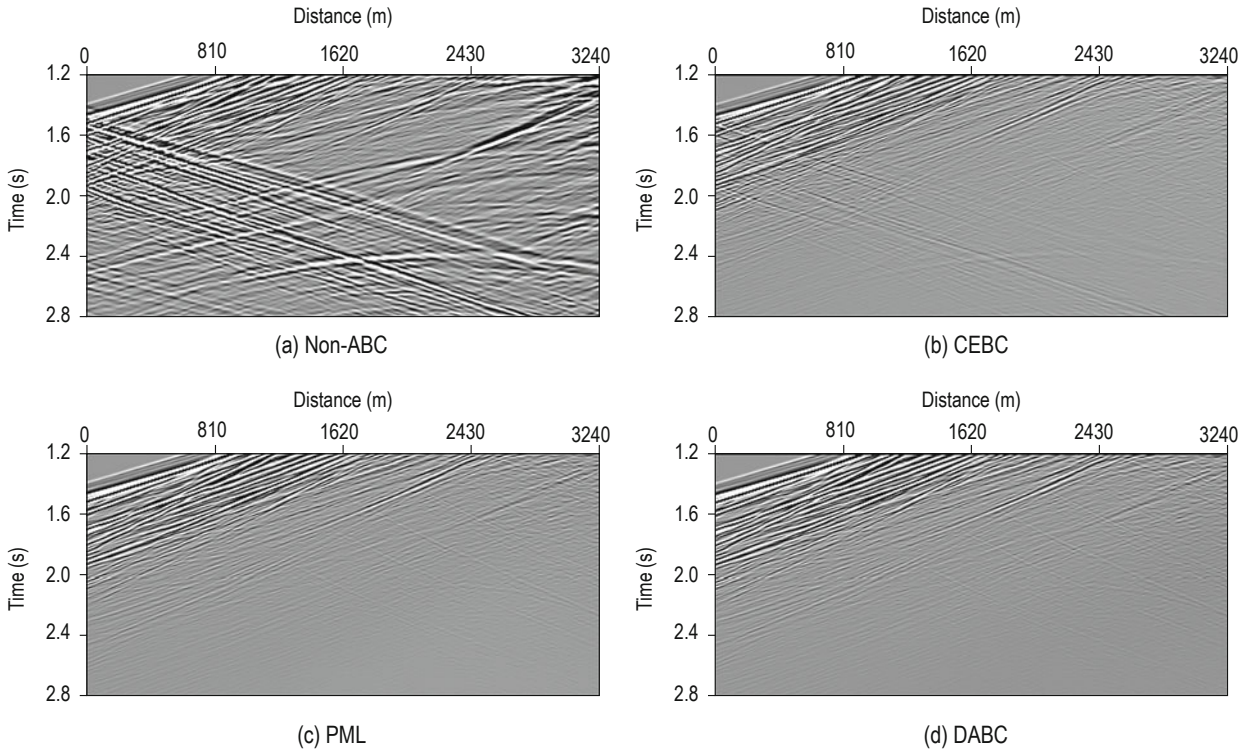

Fig.9 Partial enlargement of Figure 8.

Conclusions

We applied the DABC to seismic modeling for the first time. After analyzing the adaptability of the DABC in FD numerical modeling, we derived the particular form of the DABC by modeling the 2D acoustic wave equation and proposed specific methodological steps. Through its application to a homogeneous and a complex medium, we conclude the following.

The absorption of the DABC is clearly better than that of the CEBC and is as good as that of the PML.

The DABC does not require any modification of the wave equation when it is applied to seismic modeling. In addition, special treatmexnt of corners is avoided, which significantly reduces computational difficulties.

There are two ways to increase the absorption of the DABC. One is to widen the thickness of the boundary; the other is to increase the absorption precision. Therefore, flexibility improves.

Without the PML stability constraints, the DABC is much more stable. And finally, the DABC can be directly applied to 2D or 3D numerical modeling of the wave equation in complex media, which allows for perfect absorption. Its flexibility and stability can also facilitate subsequent inversion and migration.

References

Bécache, E., Givoli, D., and Hagstrom, T., 2010, High-order absorbing boundary conditions for anisotropic and convective wave equations: Journal of Computational Physics, **229**(4), 1099–1129.

Bérenger, J. P., 1994, A perfectly matched layer for the absorption of electromagnetic waves: Journal of Computational Physics, **114**, 185–200.

Bécache, E., Fauqueux, S., and Joly, P., 2003, Stability of perfectly matched layers, group velocities and anisotropic waves: Journal of Computational Physics, **188**(2), 399–433.

Cerjan, C., Kosloff, D., Kosloff, R., and Moshe, R., 1985, A non- reflection boundary condition for discrete acoustic and elastic wave equation: Geophysics, **50**(4), 705–708.

Clayton, R., and Engquist, B., 1977, Absorbing boundary conditions for acoustic and elastic wave equations: Bulletin of the Seismological Society of America, **67**(6), 1529–1540.

Collino, F., 1993, High order absorbing boundary conditions for wave propagation models: Straight line boundary and corner cases: Proceedings of the 2nd International Conference on Mathematical and Numerical Aspects of Wave Propagation, 161–171.

Collino, F., and Tsogka, C., 2001, Application of the perfectly matched absorbing layer model to the linear elastodynamic problem in anisotropic heterogeneous media: Geophysics, **66**(1), 294–307.

Gedney, S. D., 1996, An anisotropic perfectly matched layer-absorbing medium for the truncation of FDTD lattices: Antennas and Propagation, IEEE Transactions on, **44**(12), 1630–1639.

Givoli, D., Neta, B., 2004, High-order non-reflecting boundary scheme for time-dependent waves: Journal of Computational Physics, **186**(1), 24–46.

Hagstrom, T., Givoli, D., Rabinovich, D., and Bielak, J., 2014, The Double Absorbing Boundary method: Journal of Computational Physics, **259**, 220–241.

Higdon, R. L., 1987, Numerical absorbing boundary conditions for the wave equation: Mathematics of Computation, **49**(179), 65–90.

Komatitsch, D. and Tromp, J., 2003, A perfectly matched layer absorbing boundary condition for the second-order seismic wave equation: Geophysical Journal International, 154(1), 146–153.

Liu, Y., and Sen, M. K., 2010, A hybrid scheme for absorbing edge reflections in numerical modeling of wave propagation: Geophysics, **75**(2), A1–A6.

Liu, Y., and Sen, M. K., 2012, A hybrid absorbing boundary condition for elastic staggered-grid modeling: Geophysical Prospecting, **60**(6), 1114–1132.

Rabinovich, D., Givoli, D., and Bécache, E., 2010, Comparison of high-order absorbing boundary conditions and perfectly matched layers in the frequency domain: International Journal for Numerical Methods in Biomedical Engineering, **26**(10), 1351–1369.

Roden, J. A., and Gedney S. D., 2000, Convolutional PML (CPML): An efficient FDTD implementation of the CFS-PML for arbitrary media: Microwave and Optical Technology Letters, **27**(5), 334–339.

Song J. Y., Zheng X. D., Zhang Y., Xu J. Q., Qin Z., and Song X. J., 2011, Frequency domain wave equation forward modeling using gaussian elimination with static pivoting: Applied Geophysics, **8**(1), 60–68.

Yan, H. Y., and Liu Y., 2013a, Visco-acoustic pre-stack reverse-time migration based on the time-space domain adaptive high-order finite-difference method: Geophysical Prospecting, **61**, 941–954.

Yan, H. Y., Liu Y., 2013b, Acoustic VTI modeling and pre-stack reverse-time migration based on the time–space domain staggered-grid finite-difference method: Journal of Applied Geophysics, **90**, 41–52.

Zhao, J. G., and Shi, R. Q., 2013, Perfectly matched layer-absorbing boundary condition for finite-element time-domain modeling of elastic wave equations: Applied Geophysics, **10**(3), 323–336.

Liu Yang is a PhD student in the Department of Geological Resources and Geological Engineering, China University of Petroleum (Beijing). Her research interests are high-precision numerical modeling, physical modeling of rugged topography, and seismic processing.

(Edited by Hu Tian-Yue)